

# WMAP5 constraints on the unified model of dark energy and dark matter

T. Barreiro,<sup>1,\*</sup> O. Bertolami,<sup>2,†</sup> and P. Torres<sup>2,‡</sup>

<sup>1</sup>*Dept. de Matemática, Univ. Lusófona de Humanidades e Tecnologias  
Av. Campo Grande, 376, 1749-024 Lisboa.*

<sup>2</sup>*Departamento de Física, Instituto Superior Técnico  
Av. Rovisco Pais 1, 1049-001 Lisboa, Portugal*

(Dated: December 17, 2018)

We derive constraints on the parameter space of the unified model of dark energy and dark matter, the Generalized Chaplygin Gas (GCG), from the amplitudes and positions of the first few peaks and first trough of the cosmic microwave background radiation (CMBR) power spectrum, using the latest WMAP five year data.

PACS numbers: 98.80.-k,98.80.Cq,12.60.-i

Preprint DF/IST-1.2008

## I. INTRODUCTION

The unified model of dark energy and dark matter [1, 2, 3] is an interesting alternative to account the accelerated expansion of the universe. It is shown to be consistent with first year WMAP and other CMBR data [4, 5, 6], gravitational lensing [7], supernova data [8, 9], cosmic topology [10], gama ray bursts [11] and structure formation (see discussions in Refs. [12, 13]). The compatibility of the GCG scenario with the neutrino background radiation has been studied in Refs. [14, 15].

The GCG behavior is described by an exotic perfect fluid with the following equation of state [1, 2]

$$p_{ch} = -\frac{A}{\rho_{ch}^\alpha}, \quad (1)$$

where  $A$  is a positive constant and  $\alpha$  is a constant in the range  $0 \leq \alpha \leq 1$ . The covariant conservation of the energy-momentum tensor for an homogeneous and isotropic spacetime implies, in terms of the scale factor,  $a$ , that:

$$\rho_{ch} = \left[ A + \frac{B}{a^{3(1+\alpha)}} \right]^{\frac{1}{1+\alpha}}, \quad (2)$$

where  $B$  is an integration constant. That is, at early times the GCG behaves like non-relativistic matter, while at late times it mimics a cosmological constant. This behavior is maintained even after considering energy density perturbations [2, 3].

In this work, we update the analysis carried out in Refs. [4, 5] constraining the parameters of the GCG model. We use the bounds from the positions of the peaks and troughs of the CMBR power spectrum that

have an increased precision from the WMAP Three Year Observations and we add the bounds arising from the baryon acoustic oscillations (BAO). In this scenario we consider the GCG to be a unified dark matter/dark energy fluid with no additional cold dark matter.

We also perform a separate analysis using the full CMBR spectrum. In this case, we include an additional cold dark matter fluid, and allow for the full perturbation of the GCG fluid, following Refs. [6, 16]. We use a modified CAMB code [17] to compute the theoretical CMBR spectrum and the recently released WMAP5 Five Year Observations [18] to obtain the likelihoods. We then perform a Markov chain Monte Carlo analysis with the COSMOMC code [19], using a Metropolis algorithm, to constrain the GCG parameters.

In section II we describe the theoretical framework of our study; our results are presented in section III. Finally, our conclusions are discussed in section IV.

## II. CMBR CONSTRAINTS ON THE GCG MODEL

### A. Constraints from peak and trough locations

The CMBR peaks arise from acoustic oscillations of the primeval plasma just before the universe becomes transparent. The scale of these oscillations is set by the acoustic scale,  $l_A$ , which, for a flat universe, is given by

$$l_A = \pi \frac{\tau_0 - \tau_{ls}}{\bar{c}_S \tau_{ls}}, \quad (3)$$

where  $\tau = \tau_{ls}^{-1} \int a^{-1} dt$  is the conformal time,  $\tau_0$  and  $\tau_{ls}$  being its value at present and at last scattering respectively, while  $\bar{c}_S$  is the average sound speed before decoupling:

$$\bar{c}_S \equiv \tau_{ls}^{-1} \int_0^{\tau_{ls}} c_S d\tau, \quad (4)$$

where

$$c_S^{-2} = 3 + \frac{9}{4} \frac{\rho_b(t)}{\rho_\gamma(t)}, \quad (5)$$

\*Also at Instituto de Plasmas e Fusão Nuclear, Instituto Superior Técnico, Lisboa. Email address: tiagobarreiro@fisica.ist.utl.pt

†Also at Instituto de Plasmas e Fusão Nuclear, Instituto Superior Técnico, Lisboa. Email address: orfeu@cosmos.ist.utl.pt

‡Also at Centro de Física Teórica e de Partículas, Instituto Superior Técnico, Lisboa. Email address: torres@cftp.ist.utl.pt

with  $\rho_b/\rho_\gamma$  being the ratio of baryon to photon energy density.

In an idealized model of the primeval plasma, there is a straightforward relationship between the location of the  $m$ -th peak and the acoustic scale, namely  $l_m \approx ml_A$ . However, the peak positions are shifted by several effects which can be estimated by parametrizing the location of the  $m$ -th peak,  $l_m$ , as in Refs. [20, 21, 22]

$$l_{pm} \equiv l_A(m - \varphi_m) \equiv l_A(m - \bar{\varphi} - \delta\varphi_m), \quad (6)$$

where  $\bar{\varphi} \equiv \varphi_1$  is the overall peak shift and  $\delta\varphi_m \equiv \varphi_m - \bar{\varphi}$  is the relative shift of the  $m$ -th peak relative to the first one. Eq. (6) can also be used for the position of troughs by setting  $m = 3/2$  for the first one. We use the fitting formulae of Refs. [20, 21, 22, 23] for the shifts and the theoretical estimate of the peak locations as described in the Appendix.

The energy density, Eq. (2), can be rewritten as

$$\rho_{ch} = \rho_{ch0} \left( A_S + \frac{1 - A_S}{a^{3(1+\alpha)}} \right)^{\frac{1}{1+\alpha}}, \quad (7)$$

through the definitions  $A_S \equiv A/\rho_{ch0}^{1+\alpha}$  and  $\rho_{ch0} = (A + B)^{\frac{1}{1+\alpha}}$ . It follows for the expansion rate

$$H^2 = \frac{8\pi G}{3} \left[ \frac{\rho_{r0}}{a^4} + \frac{\rho_{b0}}{a^3} + \rho_{ch0} \left( A_S + \frac{1 - A_S}{a^{3(1+\alpha)}} \right)^{\frac{1}{1+\alpha}} \right], \quad (8)$$

where  $\rho_{b0}$  and  $\rho_{r0}$  are the baryon and radiation energy densities at present. We do not include cold dark matter in this model, its role being taken by the GCG.

It is worth mentioning that  $0 \leq A_S \leq 1$  and that, for  $A_S = 0$ , the GCG behaves as dust while for  $A_S = 1$  it behaves like a cosmological constant. The GCG model matches the  $\Lambda$ CDM model for  $\alpha = 0$  and  $A_S = 1$ .

Using the fact that  $\rho_{r0}/\rho_{ch0} = \Omega_{r0}/(1 - \Omega_{r0} - \Omega_{b0})$  and  $\rho_{b0}/\rho_{ch0} = \Omega_{b0}/(1 - \Omega_{r0} - \Omega_{b0})$ ,

$$H^2 = \Omega_{ch0} H_0^2 a^{-4} X^2(a), \quad (9)$$

where

$$X^2(a) = \frac{\Omega_{r0}}{1 - \Omega_{r0} - \Omega_{b0}} + \frac{\Omega_{b0}a}{1 - \Omega_{r0} - \Omega_{b0}} + a^4 \left( A_S + \frac{1 - A_S}{a^{3(1+\alpha)}} \right)^{\frac{1}{1+\alpha}}. \quad (10)$$

Moreover, since  $H^2 = a^{-4} \left( \frac{da}{d\tau} \right)^2$ , we get

$$d\tau = \frac{da}{\Omega_{ch0}^{1/2} H_0 X(a)}, \quad (11)$$

so that

$$l_A = \frac{\pi}{\bar{c}_S} \left[ \int_0^1 \frac{da}{X(a)} \left( \int_0^{a_{ls}} \frac{da}{X(a)} \right)^{-1} - 1 \right], \quad (12)$$

where  $a_{ls}$  is the scale factor at last scattering, for which we use the fitting formulae [20, 21, 22, 23]:

$$a_{ls}^{-1} = z_{ls} = 1048 \left[ 1 + 0.00124 \omega_b^{-0.738} \right] \left[ 1 + g_1 \omega_m^{g_2} \right], \quad (13)$$

where

$$g_1 = 0.0783 \omega_b^{-0.238} \left[ 1 + 39.5 \omega_b^{0.763} \right]^{-1},$$

$$g_2 = 0.56 \left[ 1 + 121.1 \omega_b^{1.81} \right]^{-1}, \quad (14)$$

and  $\omega_{b,m} \equiv \Omega_{b,m} h^2$ .

For the position of the peaks we consider the three year WMAP measurements, which show a considerable precision on the locations of the first two peaks and the first trough, namely [24]:

$$l_{p1} = 220.8 \pm 0.7,$$

$$l_{p2} = 530.9 \pm 3.8,$$

$$l_{d1} = 412.4 \pm 1.9, \quad (15)$$

at  $1\sigma$ .

We also consider the bound from the baryon acoustic peak [25]. Its position is related to the quantity

$$\mathcal{A} = \sqrt{\Omega_m} \left( \frac{H_0}{H(z_{lrg})} \right)^{1/3} \left[ \frac{1}{z_{lrg}} \int_0^{z_{lrg}} \frac{H_0}{H(z')} dz' \right]^{2/3}, \quad (16)$$

which takes the value

$$\mathcal{A}_0 = 0.469 \pm 0.017. \quad (17)$$

where  $z_{lrg} = 0.35$  is the redshift from the Sloan Digital Sky Survey for luminous red galaxies.

Combining Eqs. (6) and (12) and the fitting formulae of Refs [20, 21, 22, 23], shown in the Appendix, we search for the combination of GCG model parameters that is consistent with the observational bounds, taking also into account the theoretical error estimates given in the Appendix. For this analysis we fixed the value of the spectral index  $n_s = 0.963$  to the WMAP mean, and we used  $\omega_{r0} = 4.1532 \times 10^{-5}$  and  $\omega_{b0} = 0.027$  for the present energy densities of radiation and baryons respectively.

Our results are shown in section III.

## B. Likelihood analysis

Besides the peaks and trough analysis described above we also consider the full temperature and polarization spectrum to constrain the GCG model with the latest CMBR data from WMAP5. We relax our value for the cold dark matter, so that we are now really constraining a mixed model, where the GCG will be mainly responsible for the dark energy. In order to do this, we

obtain the theoretical CMBR spectrum using a modified CAMB [17] code to include the GCG evolution in the background, Eqs. (7)-(8), as well as its perturbations [16]. Using derivatives with respect to conformal time and defining the conformal time Hubble parameter,  $\mathcal{H} = a'/a$ , (where the primes denote differentiation with respect to the conformal time) we have

$$\delta' = -(1+w) \left( \theta + \frac{\dot{h}}{2} \right) - 3(c_s^2 - w)\mathcal{H}\delta, \quad (18)$$

$$\theta' = (3c_s^2 - 1)\mathcal{H}\theta + \frac{c_s^2}{(1-w)}k^2\delta, \quad (19)$$

where  $\delta$  and  $\theta$  are the density and velocity divergence perturbations for the GCG fluid, and

$$w = \frac{p_{ch}}{\rho_{ch}}, \quad (20)$$

$$c_s^2 = -w\alpha \quad (21)$$

are, respectively, the GCG fluid equation of state and speed of sound. We assume that the shear of the GCG fluid vanishes.

We included these equations into the CAMB code [17], and used the latest WMAP five year data likelihood code [18] to compute the likelihoods for this model. We used the COSMOMC [19] code to perform a Markov chain Monte Carlo analysis on our parameter space. For simplicity we fixed the inflationary input (namely, the spectral index  $n_s = 0.963$ ), and allowed changes in the parameters  $\alpha$  and  $A_S$  for the GCG fluid,  $\omega_b$  and  $\omega_c$  for the present baryon and cold dark matter energy density,  $\tau$  the optical depth and  $h$  the Hubble constant. We fixed the radiation value at the present to be  $\omega_{r0} = 4.1534 \times 10^{-5}$ . We present our results in the next section.

### III. RESULTS AND DISCUSSION

#### A. Peak and trough constraints

Fig. 1 shows the contour plots of the two first Doppler peaks and the first trough locations, as well as the baryon acoustic oscillations (BAO) peak, in the  $(\Omega_m, h)$  plane for the GCG model. Since we do not have cold dark matter in this model, the  $\Omega_m$  parameter is really an estimate of the ‘‘matter’’ component of the GCG with the baryon energy density, namely through the relation to  $A_S$  given by

$$\Omega_m = 1 - \Omega_r - A_S(1 - \Omega_b - \Omega_r). \quad (22)$$

We see that the dependance of the BAO contour on  $h$  is very slight, so the BAO constraint works as a lower bound on the value of  $\Omega_m$ . The boxes depicted in the figures are the 1-sigma bounds on  $h$  and  $\Omega_m h^2$  from the WMAP five year data fit to a  $\Lambda$ CDM model, as indicated

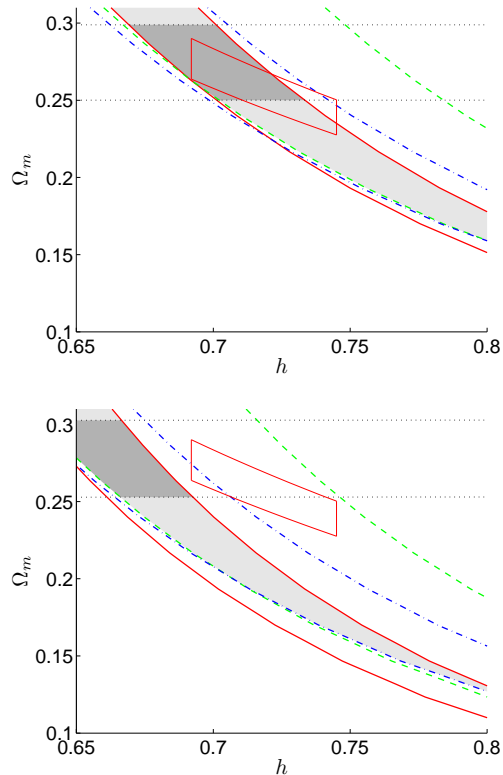


FIG. 1: Contour plots of the first two Doppler peaks and first trough locations, as well as for the baryon acoustic peak, in the  $(\Omega_m, h)$  plane for the GCG model, with  $n_S = 0.963$  for  $\alpha = 0$  (top graphic) and  $\alpha = 0.2$  (bottom figure). Full, dashed, dot-dashed and dotted contours correspond to observational bounds on  $l_{p1}$ ,  $l_{p2}$ ,  $l_{d1}$  (Eqs. (15)) and the baryon acoustic peak (Eq. (17)), respectively. The box indicates the bounds on  $h$  and  $\Omega_m h^2$  from the WMAP five year data. Darker and lighter shaded areas correspond to the allowed regions with and without BAO, respectively.

in the caption. We can see that for  $\alpha = 0$  (top figure) the results are compatible with the observations, as expected; notice also that the second peak is not measured with a sufficient accuracy to further constrain the results from the other bounds.

For  $\alpha = 0.2$  (bottom figure), we see that the BAO bound combined with the first peak bound pushes  $h$  to smaller values, making the model less viable. Higher values of  $\alpha$  are almost ruled out from the observations (see below).

Fig. 2 shows the same bounds in the  $(A_S, \alpha)$  plane. We now fix  $h = 0.719$ , still using  $n_s = 0.963$ . We see that the first peak and trough constraints allow large  $A_S$ ,  $A_S \simeq 0.9$ , and  $\alpha \lesssim 0.4$  (again, the second peak location does not noticeably change our results). Introducing the BAO constraint, however, severely affects these results, requiring  $\alpha \lesssim 0.1$  and  $A_S \simeq 0.77$ .

In comparing these results with [5], we have to consider that we are now including the estimated theoretical errors for the fitting formulae [20]. Taking this into account

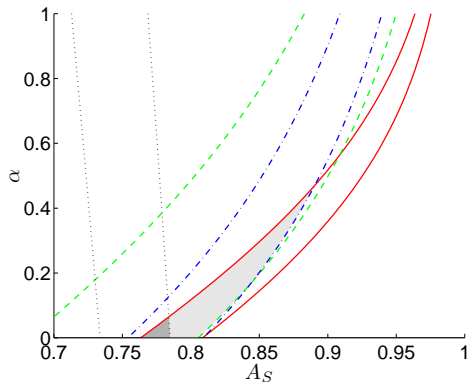


FIG. 2: Contour plots of the first two Doppler peaks and first trough locations, as well as for the baryon acoustic peak, in the  $(A_S, \alpha)$  plane for the GCG model, with  $n_S = 0.963$  and  $h = 0.719$ . Full, dashed, dot-dashed and dotted contours correspond to observational bounds on, respectively,  $l_{p1}$ ,  $l_{p2}$ ,  $l_{d1}$  (Eqs. (15)) and the baryon acoustic peak (Eq. (17)). Darker and lighter shaded areas correspond to the allowed regions with and without BAO, respectively.

shows that the new WMAP results make a considerable improvement in constraining the parameter space of the model. The BAO bounds add a significant contribution to these constraints, further reducing the allowed region of parameter values.

### B. Likelihood analysis

We start recalling that in this approach, we use the full set of perturbation equations for the GCG, so we are mainly considering the GCG fluid to act as the dark energy component. That is, we allow a separate cold dark matter energy density as a free parameter in our model.

In Figs. 3 and 4 we show the WMAP normalized power spectrum computed with CAMB. We used the WMAP five year mean values for the spectral index,  $n_S = 0.963$ , the optical depth to the last scattering surface,  $\tau = 0.087$ , and the Hubble constant,  $h = 0.719$ . We can see that the dependance of the GCG model on  $A_S$  is stronger than on  $\alpha$ . The first and second peak move to the left as we decrease  $A_S$  or as we increase  $\alpha$ , in consistency with the results from the previous sub-section. For the same parameter changes, the third peak moves to the right. The ratio between the first peak amplitude and the plateau gets smaller with decreasing  $A_S$  or increasing  $\alpha$ , due to the integrated Sachs-Wolfe effect (ISW) [6, 16]. The first and second peak intensities increase for greater values of  $A_S$  and smaller values of  $\alpha$ , while the plateau and third peak decrease. We can see that the model favours  $A_S$  values close to one and small  $\alpha$  values.

Fig. 5 shows the marginalized posterior probability densities for  $\alpha$  and  $A_S$ . We find the bounds

$$\alpha < 0.25 ,$$

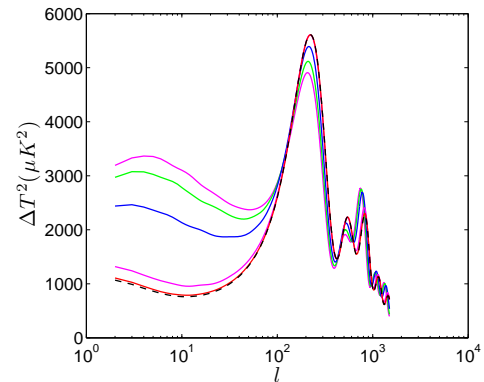


FIG. 3: The spectrum for the GCG model, compared with a  $\Lambda$ CDM model (dashed curve), for  $\alpha = 0.5$ ,  $n_S = 0.963$ ,  $\tau = 0.087$  and  $h = 0.719$ , for  $A_S = 0.7, 0.8, 0.9, 0.99, 0.999$ , from top to bottom, respectively (at the plateau).

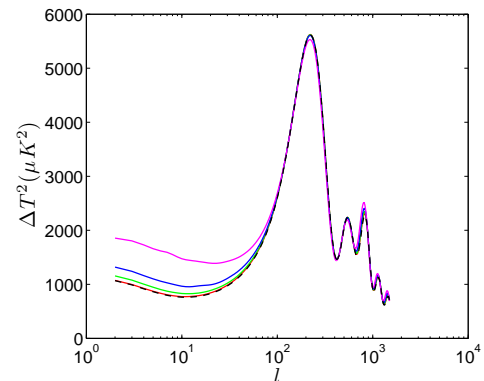


FIG. 4: The spectrum for the GCG model, compared with a  $\Lambda$ CDM model (dashed curve), for  $A_S = 0.99$ ,  $n_S = 0.963$ ,  $\tau = 0.087$  and  $h = 0.719$ , for  $\alpha = 1, 0.5, 0.2, 0.1, 0$ , from top to bottom, respectively (at the plateau).

$$0.93 < A_S < 1 , \quad (23)$$

at  $2\sigma$ .

The obtained mean values for the other parameters are  $\omega_c = 0.0935$ ,  $\omega_b = 0.0225$ ,  $\tau = 0.70$  and  $h = 0.74$ .

The difference in the bounds of  $A_S$  obtained by the previous approach and this one is easily understood. In the first case we do not consider the dark matter component, so the GCG is modeling both, dark matter and dark energy. In the second approach, dark matter is included, so the GCG contribution to this component is not the dominating one. This tends to produce a higher lower bound for  $A_S$ .

## IV. CONCLUSIONS

In the present work we have considered the position of the first two peaks and trough from WMAP three year data and other CMBR experiments that best fit WMAP

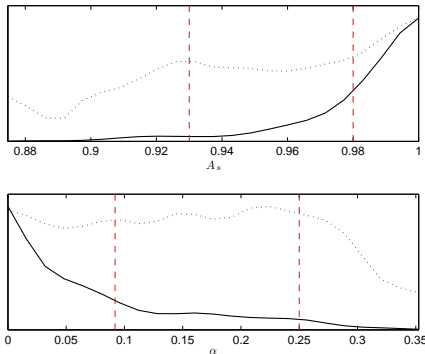


FIG. 5: Marginalized posterior probability densities for the model parameters. Dotted lines are the likelihood functions. The vertical dashed lines mark the  $1\sigma$  and  $2\sigma$  confidence levels.

five year data for  $h$  and  $n_s$ . Following the analysis of Refs. [4, 5], the new WMAP CMBR data shows that the GCG model is compatible with observations for  $\alpha \lesssim 0.4$ . The inclusion of the BAO bound further constraints the model, the allowed region of the GCG parameters being  $\alpha \lesssim 0.1$  and  $A_S \simeq 0.77$ .

Secondly, we considered the full CMBR spectrum allowing the full perturbation of the GCG fluid. We used a modified CAMB code to compute the theoretical spectrum and the COSMOMC code to perform a Markov chain Monte Carlo analysis with a Metropolis algorithm. The bound on the GCG parameters obtained were  $\alpha < 0.25$  and  $A_S > 0.93$ , at  $2\sigma$ .

### Acknowledgments

The work of T. Barreiro was partially financed by the Fundação para a Ciência e a Tecnologia (FCT, Portugal) under the grant PPD/3512/2000. The work of O.B. is partially supported by the FCT project POCI/FIS/56093/2004. The work of P.T. is fully supported by FCT under the grant SFRH/BD/25592/2005.

### APPENDIX

We have used the analytic approximations for the phase shifts found in Refs. [26, 27], which we reproduce here for convenience. The overall phase shift is given by

$$\bar{\varphi} = (1.466 - 0.466n_s) \left[ a_1 r_*^{a_2} + 0.291 \bar{\Omega}_{l_s}^{l_s} \right], \quad (\text{A.1})$$

where

$$\begin{aligned} a_1 &= 0.286 + 0.626\omega_b \\ a_2 &= 0.1786 - 6.308\omega_b + 174.9\omega_b^2 - 1168\omega_b^3 \end{aligned} \quad (\text{A.2})$$

are fitting coefficients,  $\omega_b = \Omega_b h^2$ ,

$$\bar{\Omega}_{l_s}^{l_s} = \tau_{l_s}^{-1} \int_0^{\tau_{l_s}} \Omega_{\phi}(\tau) d\tau, \quad (\text{A.3})$$

and

$$r_* \equiv \rho_{rad}(z_{ls}) / \rho_m(z_{ls}) \quad (\text{A.4})$$

is the ratio of radiation to matter at decoupling. A suitable fitting formula for  $z_{ls}$  is [27]

$$z_{ls} = 1048 [1 + 0.00124 \omega_b^{-0.738}] [1 + g_1 w_m^{g_2}], \quad (\text{A.5})$$

where

$$\begin{aligned} g_1 &= 0.0783 \omega_b^{-0.238} [1 + 39.5 \omega_b^{0.763}]^{-1}, \\ g_2 &= 0.56 [1 + 21.1 \omega_b^{-1.81}]^{-1}. \end{aligned} \quad (\text{A.6})$$

The relative shift of the first acoustic peak is zero,  $\delta\varphi_1 = 0$ , and the relative shifts of the second and third peaks are given by

$$\delta\varphi_2 = c_0 - c_1 r_* - c_2 r_*^{-c_3} + 0.05(n_s - 1), \quad (\text{A.7})$$

with

$$\begin{aligned} c_0 &= -0.1 + \left( 0.213 - 0.123 \bar{\Omega}_{l_s}^{\phi} \right) \\ &\quad \times \exp \left\{ - \left( 52 - 63.6 \bar{\Omega}_{l_s}^{\phi} \right) \omega_b \right\}, \\ c_1 &= 0.015 + 0.063 \exp(-3500 \omega_b^2), \\ c_2 &= 6 \times 10^{-6} + 0.137 (\omega_b - 0.07)^2, \\ c_3 &= 0.8 + 2.3 \bar{\Omega}_{l_s}^{\phi} + \left( 70 - 126 \bar{\Omega}_{l_s}^{\phi} \right) \omega_b, \end{aligned} \quad (\text{A.8})$$

and

$$\delta\varphi_3 = 10 - d_1 r_*^{d_2} + 0.08(n_s - 1), \quad (\text{A.9})$$

with

$$\begin{aligned} d_1 &= 9.97 + \left( 3.3 - 3 \bar{\Omega}_{l_s}^{\phi} \right) \omega_b, \\ d_2 &= 0.0016 - 0.0067 \bar{\Omega}_{l_s}^{\phi} + \left( 0.196 - 0.22 \bar{\Omega}_{l_s}^{\phi} \right) \omega_b \\ &\quad + \left( 2.25 + 2.77 \bar{\Omega}_{l_s}^{\phi} \right) \times 10^{-5} \omega_b^{-1}. \end{aligned} \quad (\text{A.10})$$

The relative shift of the first trough is given by

$$\delta\varphi_{3/2} = b_0 + b_1 r_*^{1/3} \exp(b_2 r_*) + 0.158(n_s - 1) \quad (\text{A.11})$$

with

$$\begin{aligned}
b_0 &= -0.086 - 0.079\bar{\Omega}_\phi^{ls} - (2.22 - 18.1\bar{\Omega}_\phi^{ls})\omega_b \\
&\quad - (140 + 403\bar{\Omega}_\phi^{ls})\omega_b^2, \\
b_1 &= 0.39 - 0.98\bar{\Omega}_\phi^{ls} - (18.1 - 29.2\bar{\Omega}_{l_s}^\phi)\omega_b \\
&\quad + 440\omega_b^2, \\
b_2 &= -0.57 - 3.8 \exp(-2365\omega_b^2). \tag{A.12}
\end{aligned}$$

The estimate for the accuracy of the fitting formulae is given at  $1\sigma$  by [20]:

$$\begin{aligned}
\Delta\bar{\phi} &= 0.0031, \\
\Delta\delta\phi_2 &= 0.0044, \\
\Delta\delta\phi_{3/2} &= 0.0039. \tag{A.13}
\end{aligned}$$

- 
- [1] A. Kamenshchik, U. Moshella and V. Pasquier, Phys. Lett. B **511**, 265 (2001);
- [2] M.C. Bento, O. Bertolami and A.A. Sen, Phys. Rev. D **66**, 043507 (2002).
- [3] N. Bilić, G. B. Tupper and R. D. Viollier, Phys. Lett. B **535**, 17 (2002).
- [4] M.C. Bento, O. Bertolami and A.A. Sen, Phys. Rev. D **67**, 063003 (2003); Gen. Rel. Grav. **35**, 2063 (2003).
- [5] M. C. Bento, O. Bertolami and A. A. Sen, Phys. Lett. B **575**, 172 (2003)
- [6] L. Amendola, F. Finelli, C. Burigana and D. Carturan, JCAP **0307**, 005 (2003).
- [7] P.T. Silva and O. Bertolami, Ap. J. **599**, 828 (2003); Alcaniz *et al.*, Phys Rev. D **67**, 043514.
- [8] O. Bertolami, A.A. Sen, S. Sen and P.T. Silva, Mon. Not. Roy. Astron. Soc. **353**, 329 (2004).
- [9] M.C. Bento, O. Bertolami, N.M.C. Santos and A.A. Sen, Phys. Rev. D **71**, 063501 (2005).
- [10] M.C. Bento, O. Bertolami, M.J. Rebouças and P.T. Silva, Phys. Rev. D **73**, 043504 (2006).
- [11] O. Bertolami and P.T. Silva, Mon. Not. Roy. Astron. Soc. **365**, 1149 (2006).
- [12] H. Sandvik, M. Tegmark, M. Zaldarriaga and I. Waga, Phys. Rev. D **69**, 123524 (2004).
- [13] M.C. Bento, O. Bertolami and A.A. Sen, Phys. Rev. D **70**, 083519 (2004).
- [14] A. E. Bernardini and O. Bertolami, Phys. Rev. D. **77**, 083506 (2008).
- [15] A. E. Bernardini and O. Bertolami, Phys. Lett. B **662**, 97 (2008).
- [16] R. Bean and O. Doré, Phys. Rev. D **68**, 023515 (2003).
- [17] A. Lewis, A. Challinor and A. Lasenby, Ap. J. **538**, 473 (2000)
- [18] G. Hinshaw, et.al., astro-ph/0803.0732; R. Hill, et.al., astro-ph/0803.0570; B. Gold, et.al., astro-ph/0803.0715; E. Wright, et.al., astro-ph/0803.0577; M. Nolta, et.al., astro-ph/0803.0593; J. Dunkley, et.al., astro-ph/0803.0586; E. Komatsu, et.al., astro-ph/0803.0547.
- [19] A. Lewis, S. Bridle, Phys. Rev. D **66**, 103511 (2002);
- [20] M. Doran, M. Lilley, J. Schwindt and C. Wetterich, Ap. J. **559**, 501 (2001).
- [21] W. Hu, M. Fukugita, M. Zaldarriaga and M. Tegmark, Ap. J. **549**, 669 (2001).
- [22] M. Doran, M. Lilley and C. Wetterich, Phys. Lett. B **528**, 175 (2002).
- [23] Reese et al., Ap. J. **581**, (2002) 53.
- [24] D. N. Spergel *et al.*, Ap.J. S. **170**, 377 (2007); Ap. J. S. **170**, 288 (2007).
- [25] D. Eisenstein *et al.*, Ap. J. **633**, 560 (2005);
- [26] M. Doran and M. Lilley, Mon. Not. Roy. Astron. Soc. **330**, 965 (2002).
- [27] W. Hu and N. Sugiyama, Ap. J. **471**, 30 (1996).